BigBrain – an Ultra-High Resolution 3D Human Brain Model

K. Amunts[1,2,3]*, Claude Lepage[4], Louis Borgeat[5], Hartmut Mohlberg[1], Timo Dickscheid[1], Marc-Étienne Rousseau[4], Sebastian Bludau[1], Pierre-Louis Bazin[6], Lindsay B. Lewis[4], Ana-Maria Oros-Peusquens[1], Nadim J. Shah[1], Thomas Lippert[7], Karl Zilles[1,2,3], Alan C. Evans[4]

[1] Institute of Neuroscience and Medicine (INM-1, INM-4), Research Centre Jülich, D-52425 Jülich, and JARA, Jülich-Aachen Research Alliance, Translational Brain Medicine, Germany

[2] Section Structural-Functional Brain Mapping, Dept. of Psychiatry, Psychotherapy and Psychosomatics, RWTH Aachen University, Pauwelsstr. 30, D-52074 Aachen, Germany.

[3] C. and O. Vogt Institute for Brain Research, Heinrich Heine University Düsseldorf, D-40001 Düsseldorf, Germany.

[4] Montreal Neurological Institute (MNI), McGill University, Montreal, Canada

[5] National Research Council of Canada, Ottawa, Canada.

[6] Max Planck Institute for Human Cognitive and Brain Sciences, D - 04103 Leipzig, Germany.

[7] Jülich Supercomputing Centre (JSC), Research Centre Jülich, D-52425 Jülich, Germany.

*To whom correspondence should be addressed. E-mail: k.amunts@fz-juelich.de

Reference brains are indispensable tools in human brain mapping, enabling integration of multimodal data into an anatomically realistic standard space. Available reference brains, however, are restricted to the macroscopic scale, and do not provide information on the functionally important microscopic dimension. We created an ultra-high resolution three-dimensiol (3D) model of a human brain at nearly cellular resolution of 20 micrometers, based on the reconstruction of 7404 histological sections. “BigBrain” is a free, publicly available tool that provides considerable neuroanatomical insight into the human brain, thereby allowing the extraction of microscopic data for modeling and simulation. BigBrain enables testing of hypotheses on optimal path lengths between interconnected cortical regions or on spatial organization of genetic patterning, redefining the traditional neuroanatomy maps such as those of Brodmann and von Economo.

One Sentence Summary: The first 3D-reconstructed, microscopical model of human brain architecture with a spatial resolution of 20 microns is made freely available.

Brain organization on multiple scales and regional segregation are key elements for the development of a realistic model of the human brain. Multi-scale organization requires integrating both multi-level and multi-modal data, at the level of cells with their specific connectivity, to the level of cognitive systems, and the whole brain. Magnetic Resonance Imaging (MRI) enables studying the structure and function of the living human brain with a spatial resolution in the range of 1 millimeter for structural imaging and somewhat larger for functional MRI (*1, 2*). This resolution is well above the cellular scale, but has been sufficient for establishing human brain atlases to capture information at the level of brain areas, subcortical nuclei, gyri and sulci (*2-5*). Cytoarchitectonic probabilistic maps enable the identification of microstructural correlates involved in a specific brain function as determined by functional MRI, during a cognitive task for example (*6, 7*). This is supported by combined physiological and imaging studies showing that the response properties of neurons change at the border of two areas (*8, 9*). Existing human brain atlases do not allow for the integration of information at the level of cortical layers, columns, microcircuits or cells (Fig. S1), such as has been shown recently for mouse or invertebrate brains (*10, 11*). Fine-grain anatomical resolution is a necessary prerequisite, however, to understand fully the neurobiological basis of cognition, language, emotions and other processes, and to bridge the gap between large-scale neural networks and local circuitry within the cerebral cortex and subcortical nuclei.

We sought to create a human brain model at nearly cellular resolution, going significantly beyond the 1 mm resolution of presently available atlases, taking advantage of recent progress in computing capacities, image analysis and relying on our experience in processing complete human brain histological sections. Major challenges comprise, among others, the highly folded cerebral cortex, the large number of areas, considerable inter-subject variability, and last but not least, the sheer size of the brain with its nearly 86 billion neurons, and the same number of glial cells (*12, 13*). Compared with rodent or invertebrate brains, the human brain is extremely complex: For example, the volume of the cerebral cortex is approximately 7,500 times larger, and the amount of white matter is 53,000 times larger in the human than in the mouse brain. The recently published data set of the digitized mouse brain with 1 μm resolution has a total amount of uncompressed volume data of 8 TByte (*10*). To create a volume with similar spatial resolution for the human brain would result in approximately 21,000 TByte. The interactive exploration (as opposed to simple storage) of such a dataset is beyond the capacities of current computing. Thus, among other methodological problems, data processing becomes a major challenge for any project aiming at the reconstruction of a human brain at cellular resolution.

To create the brain model, we cut a complete paraffin-embedded brain (65 year old female) coronally using a large-scale microtome (Fig. 1), acquired 7,404 sections at 20 μm thickness, and stained them for cell bodies (*14*). Histological sections were digitized, resulting in images of maximally 13,000 × 11,000 pixels (10 μm × 10 μm pixel size). The total volume of this data set was 1 TByte. Uninterrupted data acquisition time was approximately 1,000 hours. In order to generate a data set with isotropic resolution, all images were downscaled to 20 μm x 20 μm to match the section thickness of 20 μm.

Histological processing inevitably introduces artifacts, which pose problems at all stages of the 3D-reconstruction process. Defects include rips, tears, folds, missing and displaced pieces, distortion (shear), stain inhomogeneity and crystallization. Repairs were performed both manually and automatically to restore the integrity of all sections before the 3D-reconstruction of the whole brain as a contiguous volume (Figs. S2-S4). The repaired sections were registered to

the MRI, which served as an undistorted frame of reference, and further aligned section-to-section using non-linear registration. All calculations were carried out on high performance (HPC) facilities within the Compute Canada network, and run on JUROPA at the Jülich Supercomputing Centre (supporting material).

Figure 2 shows three example regions from primary sensory and motor cortices in the original coronal plane and the reconstructed sagittal and horizontal planes. Note the smooth contours in the virtual sections, confirming the high quality of the 3D-reconstruction. The images in all three planes at 20 μm reveal differences in the laminar pattern between brain areas, and enable an observer-independent definition of borders between them (*15*). To prove the feasibility of our mapping approach in higher associative cortices with more subtle architectonic differences in-between, we defined a border between Brodmann area (BA) 10 of the frontal pole and BA32 (Fig. 3). Although some artifacts due to residual mismatches between aligned sections still exist, the border of interest has been detected in the original, and the horizontal virtual plane at the identical location. Thus, the present BigBrain model allows the recognition of not only the borders between primary cortical areas (feasible, at least to some extent possible with advanced MR imaging (*16-19*)), but also between higher associative areas. Until now, the recognition of the latter borders based on their laminar pattern was accessible in 2D-histological sections and light-microscope images but only at locations where the cortex was cut orthogonal to the pial surface. The latter condition is often not fulfilled (e.g., Fig. 2A, coronal), thus making border definition based on quantitative criteria throughout the whole cortical ribbon in 2D sections impossible.

The 3D-analysis indicates that the relationship between cortical folds and borders of cytoarchitectonic areas is heterogeneous. Whereas this relationship is remarkably close for some areas, it seems to be less well defined for others. For example, the border between primary motor and somatosensory cortex is localized in the fundus of the central sulcus, independently from the orientation of the cutting plane (Fig. 2A). This is not the case for the primary auditory area Te1, which is more or less restricted by Heschl's gyrus in two planes (Fig. 2C), but has no sulcal landmark in the third plane (*20*). Whereas the sulcal pattern is associated with areal borders in other, non-primary areas, for example BA35 (*21*), the borders between the primary visual area V1 and neighboring V2 (Fig. 2B) does not seem to be related to a sulcus. The same is true for the border between BA10 and neighboring cingulate cortex (Fig. 3). This variable relationship between cytoarchitectonic borders and macroscopical landmarks has been analyzed in the past (*22, 23*), but not in 3D space.

The spatial dimension, however, is relevant, because the directionality of hemispheric growth during embryonic and fetal development and the coupling of cortical areas via fiber tracts define the spatial organization of cortical areas and their connections, as well as sulci and gyri in the adult brain. The effect of early cortical regionalization on folding has been modeled by introducing geometric, mechanic and growth asymmetries in the model (*24*). Another model considered intersubject variability during ontogeny (*25*). A recent study has emphasized the strong geometric structure of fibers and pathways as a result of early development (*26*). Another study reported that fiber connection patterns closely follow gyral folding patterns in the direction tangential to the cortical sphere (*27*). The concept of the tension-based morphogenesis effect provides a theory of folding processes caused by the tension of fiber tracts connecting brain regions (*28, 29*), whereas others identify differences in the relationship between supra- and infra-granular layers, i.e., cytoarchitectonic differences, as factors shaping cortical folding (*30*). The

validation of all these concepts requires high-resolution spatial models of the human brain for testing the underlying hypotheses.

The present findings and data on the localization of cortical areas with respect to gyri and sulci support the notion that their topographical relationship is not merely a pure geometric phenomenon, but rather the result of an interference of developmental processes and the internal structure of areas, including their connectivity (*31*). A systematic analysis of cortical borders across the whole cortical ribbon is mandatory. The variability in this relationship across individuals requires generating further BigBrain data sets in the future, labor-intensive work that is currently under way.

In order to consider intersubject variability in the present data set, vector fields have been calculated based on a 400 μm isotropic down-sampled volume, to define a homeomorphic transformation between the BigBrain and the MNI space (supporting material). Thus, cytoarchitectonic or functional probability maps in MNI space, which embeds information about intersubject variability, can be mapped to the BigBrain data set. We plan to establish links to other reference systems so as to combine high-resolution cytoarchitectonic data with, for example, gene expression maps (*32*), neural projections (*33*) or future brain activity maps (*34*).

The BigBrain dataset will be made publicly available to promote the development of novel tools for defining 3D cytoarchitectonic borders (http://bigbrain.cbrain.mcgill.ca). It allows extracting parameters of cortical organization by enabling measurements parallel to cell columns (e.g., cortical thickness, densities of cell bodies per column, surface measures) to provide a "gold standard" for calibrating in-vivo measurements of cortical thickness and other measures.

The BigBrain data set represents a new reference brain, moving from a macroanatomical perspective to microstructural resolution. This provides a basis for addressing stereotaxic and topological positions in the brain at micrometer range, e.g., with respect to cortical layers and sublayers. It will open the perspective to localize findings obtained in cellular neuroscience and mapping studies targeting transmitter receptor distributions (*35*), fiber bundles (*36*), as well as genetic data (*32, 37*). The BigBrain model can also be exploited as a source for generating realistic input parameters for modeling and simulation. It thus represents a reference frame with nearly cellular resolution, a capability that has not previously been available for the human brain, while considering the regional heterogeneity of human brain organization.

Reference List

1. P. E. Roland, K. Zilles, *Trends Neurosci.* **17**, 458 (1994).
2. A. W. Toga, P. M. Thompson, S. Mori, K. Amunts, K. Zilles, *Nat. Rev. Neurosci.* **7**, 952 (2006).
3. A. C. Evans, A. L. Janke, D. L. Collins, S. Baillet, *Neuroimage* **62**, 911 (2012).
4. P. E. Roland *et al.*, *Hum. Brain Mapp.* **1**, 173 (1994).
5. J. Talairach, P. Tournoux, *Coplanar Stereotaxic Atlas of the Human Brain* (Thieme, Stuttgart, 1988).
6. K. Zilles, K. Amunts, *Nat. Rev. Neurosci.* **11**, 139 (2010).
7. S. B. Eickhoff, S. Heim, K. Zilles, K. Amunts, *Neuroimage* **32**, 570 (2006).
8. K. Nelissen, G. Luppino, W. Vanduffel, G. Rizzolatti, G. A. Orban, *Science* **310**, 332 (2005).
9. G. Luppino, M. Matelli, R. M. Camarda, V. Gallese, G. Rizzolatti, *J. Comp. Neurol.* **311**, 463 (1991).
10. A. Li *et al.*, *Science* **330**, 1404 (2010).
11. H. Peng, Z. Ruan, F. Long, J. H. Simpson, E. W. Myers, *Nature Biotechnology* **28**, 348 (2010).
12. S. Herculano-Houzel, *Proc. Natl. Acad. Sci. U. S. A* **109 Suppl 1**, 10661 (2012).
13. C. Hilgetag, H. Barbas, *Brain Structure and Function* **213**, 365 (2009).
14. B. Merker, *J. Neurosci. Meth.* **9**, 235 (1983).
15. A. Schleicher, P. Morosan, K. Amunts, K. Zilles, *J. Autism. Develop. Disord.* **39**, 1568 (2009).
16. R. M. Sánchez-Panchuelo, S. T. Francis, D. Schluppeck, R. W. Bowtell, *J. Magn. Res. Imaging* **35**, 287 (2012).
17. G. M. Fatterpekar *et al.*, *Am. J. Neurorad.* **23**, 1313 (2002).
18. M. F. Glasser, D. C. Van Essen, *J. Neurosci.* **31**, 11597 (2011).
19. N. B. Walters *et al.*, *Hum. Brain Mapp.* **28**, 1 (2007).
20. P. Morosan *et al.*, *Neuroimage* **13**, 684 (2001).
21. J. C. Augustinack *et al.*, *Neuroimage* **64**, 32 (2013).
22. K. Amunts *et al.*, *Neuroimage* **22**, 42 (2004).
23. B. Fischl *et al.*, *Cereb. Cortex* **18**, 1973 (2007).
24. R. Toro *et al.*, *Cereb. Cortex* **18**, 2352 (2008).
25. J. Lefevre, J. F. Mangin, *PLoS. Comput. Biol.* **6**, e1000749 (2010).

26. V. J. Wedeen *et al.*, *Science* **335**, 1628 (2012).

27. H. Chen *et al.*, *Cereb. Cortex* (2012).

28. D. C. van Essen, *Nature* **385**, 313 (1997).

29. A. Kriegstein, S. Noctor, V. Martinez-Cerdeno, *Nat. Rev. Neurosci.* **7**, 883 (2006).

30. E. Armstrong *et al.*, *Cereb. Cortex* **1**, 426 (1991).

31. K. Zilles, K. Amunts, *Science* **335**, 1582 (2012).

32. A. R. Jones, C. C. Overly, S. M. Sunkin, *Nat. Rev. Neurosci.* **10**, 821 (2009).

33. N. Kasthuri, J. W. Lichtman, *Nat. Methods* **4**, 307 (2007).

34. A. P. Alivisatos *et al.*, *Science* (2013).

35. K. Zilles, K. Amunts, *Curr. Opin. Neurol.* **22**, 331 (2009).

36. M. Axer *et al.*, *Frontiers in Neuroinformatics* **5**, 1 (2011).

37. E. H. Shen, C. C. Overly, A. R. Jones, *Trends in Neurosciences* **35**, 711 (2012).

38. Acknowledgements. We wish to acknowledge funding support from CANARIE (www.canarie.ca) for the software development of the CBRAIN portal. We also wish to thank Compute Canada (https://www.computecanada.ca) for its continued support through extensive access to the Compute Canada HPC grid. We thank Patricia Morosan and Uwe Pietrzyk for helpful discussion, as well as Ferdag Kocaer and Ursula Blohm for technical assistance. We are particularly grateful to Reza Adalat for his efforts in management and coordination on this collaboration. This project was supported by the Portfolio project "Supercomputing and Modelling the Human Brain", funded by the Helmholtz Association Germany. It is a preparatory project for the EU flagship "Human Brain Project".

Fig. 1. Illustration of tissue and image processing. (A) Photographs of the fixed brain; lateral left, lateral right and dorsal views. (B) MR image (coronal view) and (C) 3D-reconstructed MRI volume of the fixed brain. (D) Histological sectioning. (E) Blockface image of a section (pseudo-colored) resting on the mounting grid that served for alignment of the blockface images. (F) Series of blockface images. (G) Cell-body stained histological sections with region-of-interest, which is shown with higher magnification in (H). (I) Series of histological images, which were 3D-reconstructed using the blockface images (F) and the MRI (C).

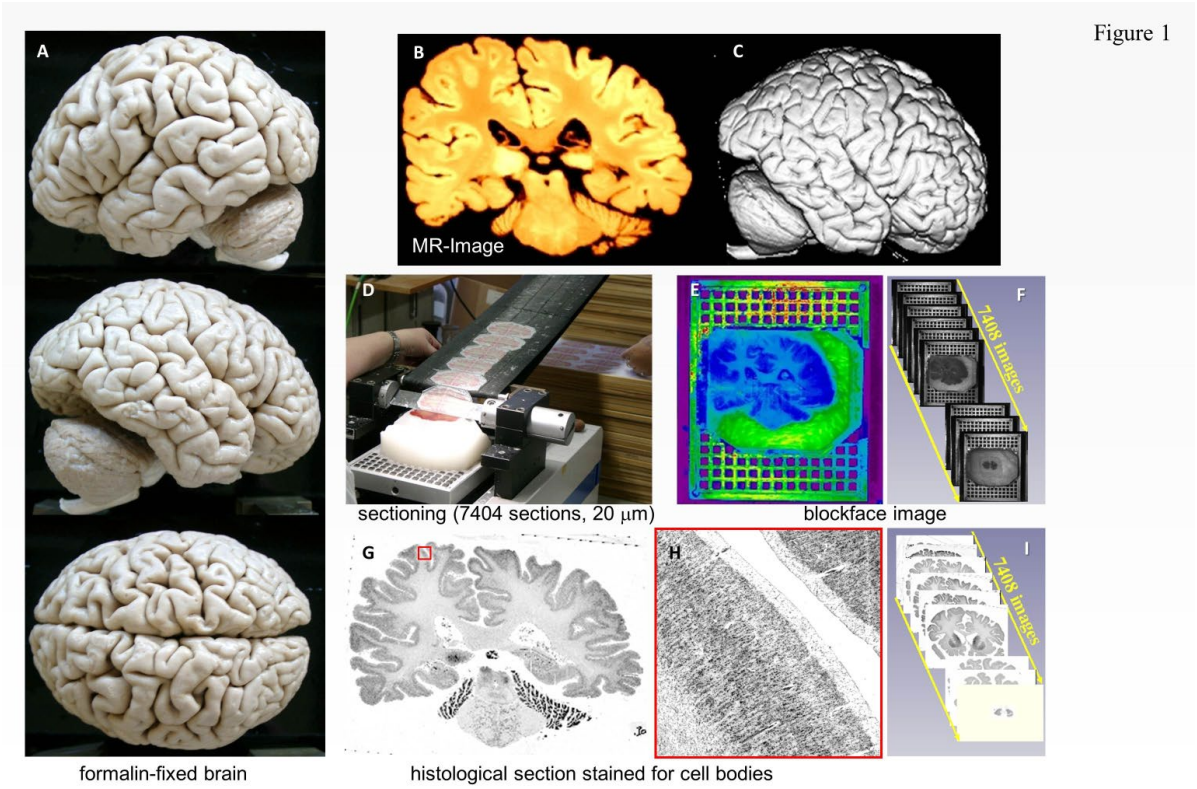

Fig. 2. Primary cortical regions in the three planes of section: (A) sensorimotor (BA 4, 3a&b), (B) visual (areas v1, v2), and (C) auditory cortex (areas Te1.0, Te1.1). Left column: overviews of the whole brain sections in the original plane (A), and the 3D-reconstructed horizontal (B) and sagittal (C) planes. Cross hairs label identical positions within a row. Columns I-III: coronal, sagittal, and horizontal planes, respectively. *cs* – central sulcus, HG – Heschl's gyrus. Section numbers in left lower corner. (D-G) definition of borders for ROIs from (A-C) based on the Mahalanobis distance (*15*); corresponding borders are labeled by identically colored arrows (see also supporting material and Fig.3). Yellow crosshairs indicate identical positions in each ROI.

Figure 2

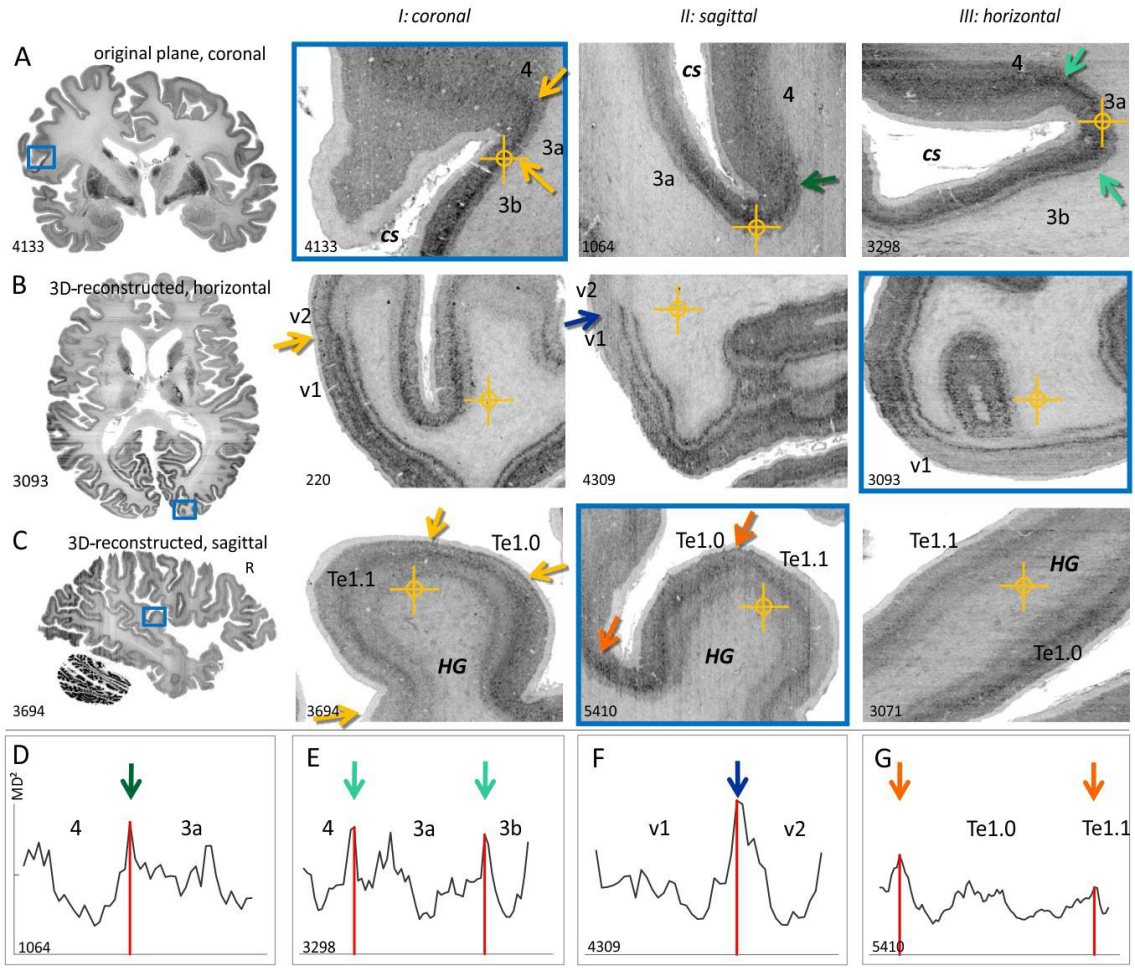

Fig. 3 Definition of a boundary (*15*) in the frontal cortex. (A) Surface rendering of the 3D-reconstructed brain from rostral with the frontal pole removed. (B) Coronal section #6704. (C) 3D-reconstructed horizontal (#2740) and (D) sagittal (#3588) sections. Yellow crosshairs at identical position in A-F. (E-J) Border definition in sections (B) and (C). Green: mean profile of mesial BA10, blue: mean profile BA32 (E,F). (G,H) Mahalanobis distance as a function of position along the cortical profile. (I,J) Localization of significant peaks in the Mahalanobis distance (see supporting material).